# In-Home Power Line Communication Channel: Statistical Characterization

A. M. Tonello, *Senior Member, IEEE,* F. Versolatto, *Student Member, IEEE,* and A. Pittolo

*Abstract*—A statistical characterization of the in-home power line communication channel is performed from the study of a wide set of measured channels in the 1.8–100 MHz frequency band. The study provides new insights on a) the relation between the line impedance and the channel frequency response (CFR), b) on the spatial relation between the channels that share either the transmitter or the receiver outlet. Furthermore, it confirms the validity of some results presented in the literature that are limited to the 30 MHz band. The study comprises the analysis of the average channel gain, the root-mean-square delay spread and the coherence bandwidth, as well as the relation between such quantities and the phase of the CFR. Closed-form expressions are provided to model the quantities and their relations. Finally, the coverage, i.e., the relation between the maximum achievable rate and the distance, as well as the achievable rate gain offered by the use of the frequency band up to 300 MHz, are studied.

*Index Terms*—Power line communications channel, channel characterization, broadband PLC, fading, spatial correlation.

## I. INTRODUCTION

IN recent years, power line communications (PLC) have gained success as a valuable solution to deliver high-speed multimedia content through the existent wiring infrastructure.

The idea of using the power delivery network for communication purposes dates back to 1918. Initially, PLC were intended for command and control applications over high and medium voltage lines [1]. Nowadays, the use of advanced modulation schemes, as orthogonal frequency division multiplexing, enables communications up to 1 Gbps at the physical layer, as, for instance, specified by the HomePlug AV2 standard [2]. Further improvements require the detailed knowledge of the communication medium. The variability of the wiring structures translates into an extreme variability of the PLC channel. Line discontinuities and unmatched loads generate multipath fading effects [3]. In this respect, the statistical characterization of the PLC channel is fundamental.

In the literature, a lot of effort has been spent on this topic. A first characterization of the PLC channel was presented in [4]. The study was based on measurements up to 60 MHz. In [5], the feasibility of high-speed PLC was tested for the in-home US scenario. The test was carried out with prototype devices in the 1.8–30 MHz frequency range, namely, that deployed by most of broadband PLC commercial systems. New standards enable communications up to 60 MHz, e.g., IEEE P1901 [6], and even beyond 100 MHz, e.g., ITU-T G.hn [7].

A characterization of the PLC channel up to 100 MHz was presented in [8]. The analysis was based on a measurement campaign that was performed in France and it yielded the classification of the channels into nine classes according to the channel capacity. In [9], the classes were described in terms of associated root-mean-square (RMS) delay spread and coherence bandwidth (CB). More recently, in [10], it was shown that the RMS delay spread is negatively related to the average channel gain (ACG). This result was confirmed in [11], where the statistics of the PLC channel was further compared to that of phone lines, coaxial cables and medium voltage lines. Both [10] and [11] targeted the 1.8–30 MHz frequency band. An analysis of the RMS delay spread, the ACG and the normality of the CFR in dB of a set of measured channels was also reported in [12]. The database consists of 200 measures and the measurements were performed in Spain. All previous contributions address the in-home PLC scenario, with the exception of [11] that also considers medium voltage and phone lines.

The former results are not strictly comparable because of some differences. For instance, [8] considers the bands 0.03–100 MHz and 2–100 MHz, [10] and [11] the band 1.8–30 MHz, and [12] the band 2–30 MHz. Furthermore, the method used to compute the impulse response is not always detailed. Thus, it is rather difficult to replicate the measurement setup and to compare the results in terms, for instance, of RMS delay spread. In this paper, we aim to provide a detailed procedure for the computation of the physical quantities (metrics) that characterize the channel from the measurements in the frequency domain. Hence, we present the statistical analysis of a large set of in-home PLC channels that were measured in Italy. The results are compared to those provided in the literature, highlighting, when necessary, the differences in the setup. The focus is on the frequency band 1.8–100 MHz because this is the band of interest of current and next-generation PLC standards. A further analysis beyond 100 MHz and up to 300 MHz is provided in order to quantify the potentiality in terms of achievable rate improvement.

The final goal of this characterization work is to provide new information about the PLC channel in order to foster the refinement of the existent models that either follow a top-down or a bottom-up approach. In fact, the literature reports a variety of PLC channel models. Among the ones that follow a top-down approach, a multipath propagation model was firstly proposed in [13], than improved in [3], and finally extended in statistical terms in [14]. Alternative top-down channel models were discussed in [8] and [15]. Indeed, a larger number of bottom-up channel models exist. First attempts were discussed in [16] for the in-home scenario, and in [17] for the narrowband outdoor low-voltage scenario. More recently, bottom-up models based on the *s*-parameters, transmission/reflection

The authors are with the Department of Electrical, Mechanical and Management Engineering (DIEGM), University of Udine, Udine 33100, Italy (e-mail: {tonello, fabio.versolatto, alberto.pittolo}@uniud.it).

coefficients, wavelet expansion of $s$-parameters and ABCD-matrix representations were presented in [18], [19], [20], and [21], respectively. Grounding practices, typical of the US scenario, were modeled in [22], while a channel generator obtained combining a random topology generation algorithm and an efficient channel response computation method was detailed in [23]. Finally, the channel time-variance was studied and modeled in [24] and references therein.

We collected a database of 1266 channel responses in different premises, and we performed measurements in the frequency domain up to 300 MHz. Some preliminary results of the analysis were reported in [25], [26]. Namely, in [25], the relation between the channel statistics and the physical distance between the transmitter and the receiver outlet was presented. The work focused on the 2–100 MHz frequency band. Indeed, in [26], some partial results on the statistics of the channel response and the line impedance were discussed. In this paper, a more comprehensive analysis and a reconciliation of previous results is reported. Compared to previous contributions, the main advances to the knowledge of the PLC channel in this work can be summarized as follows.

- The statistics of the amplitude of the CFR is studied up to 100 MHz. The distribution that fits best (among the known ones) the measured CFR amplitude is studied, and a closed-form expression of the mean and the standard deviation of the distribution is provided as a function of frequency.
- The ACG, the RMS delay spread, the CB and their relation is studied in the band 1.8–100 MHz. The main findings concern the impact of the method used to compute the channel impulse response (CIR) on the statistics of the RMS delay spread, and the relation between the ACG and the RMS delay spread. The relation between the phase slope of the CFR and both the ACG and the RMS delay spread is reported. Furthermore, two CB definitions are presented and referred to as statistical and deterministic CB. They are obtained from the study of different correlation functions of the CFR. The introduction of the statistical CB is motivated by the work in [14], where the quantity is exploited to fit a top-down model.
- The spatial correlation, i.e., the correlation between the channels belonging to different outlet pairs, is investigated. Several quantities are considered, i.e., the correlation between channels of the same site, the correlation between the channels that share the same transmitter outlet, and the correlation between the channels that share the same receiver outlet. To remove the randomization due to the phase, the last two quantities are evaluated when the amplitude correlation of the channel frequency response is considered.
- The relation between the CFR and the line impedance is investigated. A method to determine the high probability regions in their scatter plot is detailed.
- The dependencies of the maximum achievable rate on the frequency band and on the distance between the end nodes are shown. In this respect, it should be noted that the distance is defined in terms of difference between

the position of the transmitter and receiver outlet, and, in general, it does not match with the length of the path followed by wirings.

- In order to facilitate the comparison of the measured data, and following the spirit of replicable research, closed-form expressions are provided to model the statistical quantities and their relations. Furthermore, a script is made available on-line [27]. The script computes the CIR and the main statistical metrics from the measure of the CFR. The aim is to share a common tool that may allow for future comparisons.

The analysis that follows is time-invariant. The PLC channel exhibits, in general, a linear and periodically time variant behavior [28], but, from the experimental observations, we found that the time-dependency is not pronounced in the considered frequency band. This finding is validated by other experimental results, e.g., [29], where it is shown that channel time variations are mostly experienced below 2 MHz.

The remainder of the paper is organized as follows. Section II describes the measurement campaign. Section III deals with the definition of the channel response, the line impedance and it presents the procedure to compute the channel impulse response. Section IV describes the statistical metrics that are considered in the following. Then, in Section V, the results of the characterization activity are presented. Finally, the conclusions follow.

## II. Measurement Campaign

We performed an experimental campaign in Italy, on single-phase in-home networks. Three sites were considered as representatives of small flats and detached houses of the urban and suburban scenario. The area of the sites ranges between 50 and 200 m². For each site, all the available outlets were considered to provide a comprehensive view. In this respect, we did not limit the set of outlets to those that were considered most probable for a PLC transmission, as for instance, it was done in [8].

Measurements were carried out in the frequency domain, with an Agilent E5061B VNA. The transmit power was set to 10 dBm. To protect the equipment from the mains, couplers were used and extension cables with characteristic impedance of 50 $\Omega$ enabled to assess distant outlets. The couplers are broadband high-pass filters and they exhibit an attenuation lower than 5 dB up to 100 MHz. The effect of the couplers and cables was removed by measuring first their ABCD matrix and then deconvolving them from the overall measurement.

For each channel, 16 subsequent acquisitions were averaged to obtain the actual scattering ($s$) parameters. From experimental observations, 16 acquisitions were sufficient to cope with noise impairments. From the $s$-parameters, the CFR, and the line impedance were obtained. In the following, the superscript $\{\cdot\}^i$ denotes the $i$-th acquisition, where $i = 1, \ldots, \mathcal{I}$ and $\mathcal{I} = 1266$. A discrete-frequency representation is used according to the fact that the VNA acquires a finite number of points regardless the frequency span. The index $m$ denotes the frequency sample $f = m\Delta f$, where $\Delta f$ is the resolution in frequency. Unless otherwise stated, the start and

stop frequency are denoted with $M_1\Delta f = f_1 = 1.813$ MHz and $M_2\Delta f = f_2 = 100$ MHz, where $\Delta f = 62.5$ kHz, $M_1 = 29$ and $M_2 = 1600$. Acquisitions beyond 100 MHz and up to 300 MHz were also done as discussed in Section V-E. In this case, $f_1 = 1.875$ MHz, $\Delta f = 187.5$ kHz, $M_1 = 10$ and $M_2 = 1600$.

## III. CHANNEL RESPONSE AND LINE IMPEDANCE

The CFR is defined as the ratio between the voltage at the receiver outlet and the voltage at the transmitter outlet. The line impedance is the ratio between the voltage and the current at the transmitter port when the receiver is connected to a 50 $\Omega$ load, i.e., the characteristic impedance of the cables that were deployed and the reference impedance of the VNA. $H(m)$ and $Z(m)$ denote the CFR and the line impedance, respectively. Furthermore, $R(m)$ and $X(m)$ denote the real and the imaginary component of $Z(m)$, respectively.

### A. Channel Impulse Response

The channel impulse response is obtained from the CFR by means of processing, i.e., by windowing the CFR, applying an inverse discrete Fourier transform (IDFT), and truncating the less significant tails. In detail, the procedure that we adopt is the following.

- Let us focus on the CFR in the frequency range from 0 to $f_2$. The CFR is defined in the discrete-frequency domain and the number of CFR samples is $M_2 + 1$. From 0 to $f_1$, the CFR is set equal to zero.
- Let us compute the IDFT of the CFR to obtain the real CIR at time instant $t = nT$, namely, $h(n)$, where $n = 0, \ldots, N$, $N = 2M_2$, and $T$ is the resolution in time. The CIR is defined in the discrete time domain with temporal resolution $\Delta t = 1/[(N + 1)\Delta f]$.
- To cut the tails introduced by the IDFT we proceed as follows. Firstly, let us shift the pulse in order to bring the anti-causal tails introduced by the IDFT to the beginning of the CIR. Then, let us compute the normalized cumulative pulse energy as $E(n) = \sum_{k=0}^{n} |h(k)|^2 / \sum_{k=0}^{N} |h(k)|^2$. Finally, let us set $h(n) = 0$ $\forall n$ subject to $E(n) \leq (1-\alpha)/2$, $E(n) \geq \alpha + (1-\alpha)/2$. In the following analysis the value $\alpha = 0.98$ is used.

The definition of a detailed procedure is motivated by the fact that processing affects the results and, in turn, the statistics of the metrics that are computed from the CIR. As an example, Table I reports the minimum, mean and maximum value of the RMS delay spread (see Section IV-B) computed from impulse responses obtained with different processing procedures. As it can be noted, the RMS delay spread becomes larger when the bandwidth decreases. Furthermore, as intuition suggests, the RMS delay spread decreases when less channel energy is accounted by the CIR due to the tail cut operation ($\alpha$ factor). In this respect, the case $\alpha = 1$ shows that the side lobes introduced by the rectangular window applied in frequency corrupt the RMS calculation.

## IV. CHANNEL STATISTICS

Herein, the definition of ACG, RMS delay spread, CB and maximum achievable rate is reported. In the following, the relation between the metrics and the distance is also studied. The distance is the euclidean norm between the coordinates of the transmitter and the receiver outlet and, in general, it does not correspond to the length of the cables that connect pairs of outlets. Finally, the spatial correlation among channels is discussed.

### A. Average Channel Gain

The ACG is a scalar metric that describes the average attenuation (averaged along frequencies) of the channel. For each acquisition $i$, the ACG in dB-scale reads

$$G^i = 10 \log_{10} \left( \frac{1}{M_2 - M_1} \sum_{m=M_1}^{M_2} |H^i(m)|^2 \right) \quad \text{[dB]}, \quad (1)$$

where $H^i(m)$ is the $i$-th acquired CFR at frequency $m\Delta f$. In [12], an alternative definition of the ACG is provided as the mean of the dB-version of the CFR. From the literature, the ACG is expected to be normally distributed [10].

### B. RMS Delay Spread

The RMS delay spread accounts for the energy dispersion of the CIR. It reads

$$\sigma_\tau = \sqrt{\sum_{n=0}^{N} (nT)^2 \mathcal{P}(nT) - \left( \sum_{n=0}^{N} nT \mathcal{P}(nT) \right)^2} \quad \text{[s]}, \quad (2)$$

where $\mathcal{P}$ is the power delay profile, defined as $\mathcal{P}(nT) = |h(nT)|^2 / \sum_{n=0}^{N} |h(nT)|^2$. In the literature, it has been shown that the RMS delay spread of the PLC channel can be modeled as a log-normal random variable [10]. From the experimental observations, in Section V, the validity of such a model is confirmed.

### C. Coherence Bandwidth

The coherence bandwidth can be defined starting from two different correlation functions. A first approach is to use the

TABLE I
AVERAGE RMS DELAY SPREAD FOR DIFFERENT TRANSMISSION BANDS
AND THRESHOLD COEFFICIENTS

| Band (MHz) | $\alpha$ | $\sigma_\tau$ ($\mu$s) | | |
|---|---|---|---|---|
| | | min | mean | max |
| 0–30 | 1 | 0.133 | 1.257 | 5.360 |
| | 0.98 | 0.030 | 0.942 | 5.294 |
| | 0.9 | 0.008 | 0.574 | 5.002 |
| 1.8–30 | 1 | 0.114 | 0.581 | 1.825 |
| | 0.98 | 0.033 | 0.394 | 1.524 |
| | 0.9 | 0.012 | 0.278 | 0.957 |
| 0–100 | 1 | 0.114 | 1.153 | 5.284 |
| | 0.98 | 0.018 | 0.842 | 5.210 |
| | 0.9 | 0.002 | 0.500 | 4.909 |
| 1.8–100 | 1 | 0.056 | 0.502 | 1.613 |
| | 0.98 | 0.017 | 0.337 | 1.280 |
| | 0.9 | 0.001 | 0.239 | 0.926 |

correlation function of the CFR as formally done in [30]:

$$\phi(\ell, m) = \frac{E_i[H^i(\ell)\left(H^i(m)\right)^*]}{\sqrt{E_i[|H^i(\ell)|^2]E_i[|H^i(m)|^2]}}, \qquad (3)$$

where $\ell$ and $m$ denote the frequencies, and $E_i[\cdot]$ and $\{\cdot\}^*$ denote the expectation operator (across channel realizations, $i$) and the complex conjugate, respectively. In the presence of uncorrelated scattering, which is a typical situation in wireless communications, $\phi(\ell, m)$ is a function of the difference $\Delta = \ell - m$. In PLC this does not apply, therefore similarly to [14], we can define the averaged correlation function

$$\overline{\phi}(m) = \Delta f \sum_{\ell=M_1}^{M_2} \phi(\ell, m). \qquad (4)$$

Now, the CB at level $\rho$, $\hat{B}_c^\rho$, is the frequency for which the absolute value of $\overline{\phi}(m)$ falls below $\rho$ times its maximum, i.e.,

$$\hat{B}_c^\rho = B \quad \text{s.t.} \quad |\overline{\phi}(B)| = \rho|\overline{\phi}(0)|. \qquad (5)$$

Another approach is to compute the correlation of each channel frequency response as

$$R^i(m) = \Delta f \sum_{\ell=M_1}^{M_2} H^i(m+\ell)\left(H^i(\ell)\right)^*, \qquad (6)$$

where $H^i(m) = 0$ outside $[f_1, f_2]$. Differently from (3), (6) is specific to a given channel realization and it is only a function of the frequency difference $m$. Therefore, we refer to it as deterministic correlation. For a given channel $i$ we can compute its CB, namely, $B_c^{\rho,i}$, as in (5) by substituting $\overline{\phi}(m)$ with $R^i(m)$. Finally, the average CB, $\overline{B}_c^\rho$, is obtained by averaging $B_c^{\rho,i}$ across the ensemble of channels, namely, $\overline{B}_c^\rho = E_i\left[B_c^{\rho,i}\right]$.

In order to distinguish them, we refer to statistical CB when the first approach is used, while to deterministic CB when the second approach is used. The statistical CB was used to fit the model in [14] to the measures. Some experimental works, e.g., [9], deal with the deterministic CB because the number of acquisitions does not allow for computing the expectation in (3). A numerical comparison between $\hat{B}_c^\rho$ and $\overline{B}_c^\rho$ is reported in Section V-C.

### D. Maximum Achievable Rate

Under the assumption of additive colored Gaussian noise, the Shannon capacity of the $i$-th channel reads

$$C^i = \Delta f \sum_{m=M_1}^{M_2} \log_2 \left(1 + \frac{P_{tx}(m)\left|H^i(m)\right|^2}{P_w(m)}\right) \quad \text{[bps]}, \quad (7)$$

where $P_{tx}(m)$ and $P_w(m)$ are the power spectral density (PSD) of the transmitted signal and of the noise at frequency $m$, respectively. The maximum achievable rate is widely deployed in the literature, though in most of the cases, simplified noise models are used. In [8] and [11], the noise is assumed to be white, with a PSD of -140 dBm/Hz and -120 dBm/Hz, respectively. Some other papers account for the colored nature

of the noise. We adopt the additive colored Gaussian noise model presented in [31]. Namely, the noise PSD reads

$$P_w(m) = 10\log_{10}\left(\frac{1}{(m\Delta f)^2} + 10^{-15.5}\right) \quad \text{[dBm/Hz]}. \quad (8)$$

It should be noted that, since there are several noise disturbances whose statistical characterization has not been thoroughly done yet, the true PLC channel capacity may be overestimated by (7) according to the noise model in (8). More in detail, we do not account for the contribution due to narrowband and FM broadcast radios. For the numerical analysis, the transmitted PSD will be set equal to -55 dBm/Hz up to 30 MHz, and equal to -80 dBm/Hz beyond 30 MHz. The PSD reduction above 30 MHz is required to fulfill with EMC requirements [32].

### E. Spatial Correlation

PLC channels associated to different pairs of outlets of the same site may share part of the signal path because the propagation takes place on the same electrical circuit. Thus, they are supposed to experience similar reflection effects. In this respect, we aim to verify whether channels of the same site, or that share the transmitter or the receiver outlet, are correlated. This information is fundamental when more than two nodes are involved in the communication, e.g., to study realistic multiple user schemes or relaying techniques. We analyze the space-frequency correlation that is formulated in a similar manner to (3), as follows

$$\psi(\ell, m) = \frac{E_{i,j}\left[H^i(\ell)\left(H^j(m)\right)^*\right]}{\sqrt{E_i\left[|H^i(\ell)|^2\right]E_j\left[|H^j(m)|^2\right]}}, \qquad (9)$$

where $i \neq j$, and the expectation in $i, j$ is across the channel realizations of the same site.

Due to the large heterogeneity of in-home channels (signal paths), we expect (9) to be small. This has been verified experimentally (see Section V-D). To limit the variability and get useful information, we propose to focus only on the channels that share the same transmitter outlet or the same receiver outlet. This is representative of the broadcast downlink case, and of a case where multiple transmitters, e.g., video cameras, send data to a concentrator, respectively. We denote with $\psi_x(\ell, m)$, $x = t, r$, the correlation of the CFR between frequencies $\ell$ and $m$ for the channels that share the same transmitter outlet, i.e., $x = t$, and for channels that share the same receiver outlet, i.e., $x = r$. Then, we compute $\psi_x(\ell, m)$ as in (9), but limiting the expectation over the channels in $i, j$ that share the same transmitter outlet for $\psi_t$ and over channels that share the same receiver outlet for $\psi_r$. In particular, we limit the study to $\ell = m$, i.e., $\psi_x(m) = \psi_x(m, m)$.

The numerical results will show that the spatial correlation assumes low values. We speculate that this is because of the random contribution of the phase of distinct channels which is uniformly distributed in $(-\pi, \pi)$. Therefore, we also study the correlation $\psi_{x,abs}(f)$ that is defined as $\psi_x(f)$, with $x = t, r$, but considering the absolute value of the CFRs, i.e., $|H^i(\ell)|$, $|H^j(m)|$, in the expectation at the numerator of (9).
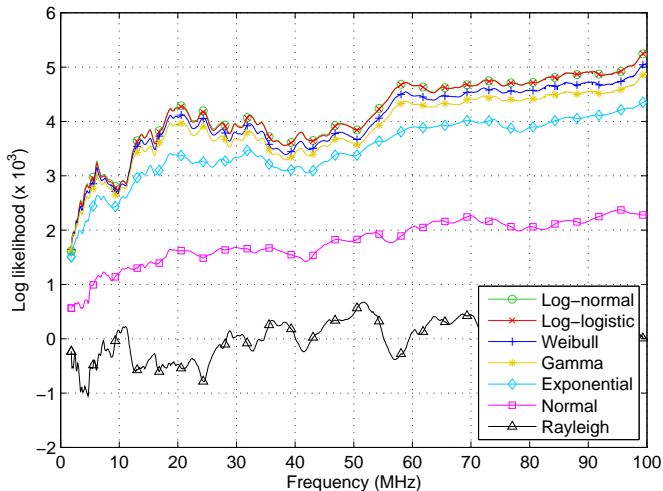
Fig. 1. Log-likelihood value of the best fitting of the measured CFR amplitude for different distributions.
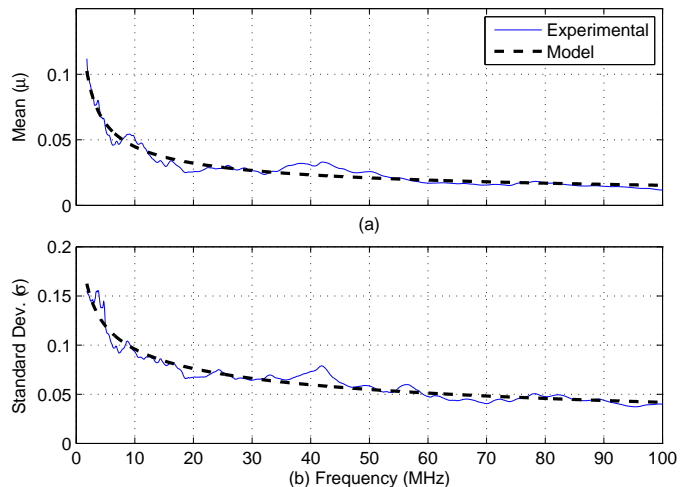


Fig. 2. Experimental mean and standard deviation of the best Log-normal fit of the measured CFR amplitude (in linear scale) as a function of frequency. The model of both quantities is also shown.

## V. CHANNEL CHARACTERIZATION

In this section, we report the results of the characterization of the channel using the metric definitions of the previous section. Unless otherwise specified, the study is limited to the frequency range between 1.8 and 100 MHz, namely, the band of interest of current and next generation PLC systems.

### A. Channel Frequency Response

Herein, we study the distribution of the amplitude of the CFR in linear scale. We fit the distribution of the measured amplitude with the following well known distributions: Exponential, Gamma, Log-normal, Normal, Rayleigh, Weibull and Log-logistic. Basically, for each distribution, we obtain the maximum likelihood estimates of the distribution parameters. Hence, we compute the likelihood function [33, Chap. 2]

$$\Lambda(\theta) = \prod_{x \in \mathbb{X}} p(x|\theta), \qquad (10)$$

where $x \in \mathbb{X}$ is the set of measured samples, $p(\cdot)$ is the probability density function (PDF) of the fitting distribution, and $\theta$ represents the parameters of the fitting distribution that were obtained by the estimation. The higher the likelihood function in (10), the better the parameters fit the measured distribution. We neglect the limits of (10) when dealing with models with different complexities, namely, that are described with a different number of parameters.

The analysis is performed as a function of frequency, and Fig. 1 reports the value of the logarithmic version of (10) obtained with the set of the distribution parameters that yields the best fit. The Log-normal distribution provides the highest likelihood value almost in the entire frequency range, i.e., a result that was already mentioned in [26]. Only the few low frequencies between 1.8 and 2 MHz are better fitted by the Weibull distribution, which gets a slightly higher score. Therefore, as a main conclusion, the measured data, in dB scale, is normally distributed as reported formerly in [10], and validated in [26].

Fig. 2, shows the mean $\mu$ and the standard deviation $\sigma$ of the best Log-normal fit of the channel amplitude in linear scale as a function of frequency. Both quantities exhibit an exponentially decreasing behavior that can be modeled as follows $\lambda(m) = a_\lambda m^{b_\lambda} + c_\lambda$, where $\lambda$ is the parameter ($\mu$ or $\sigma$), and $a_\lambda$, $b_\lambda$, and $c_\lambda$ are constant coefficients. Table II reports the value of $a_\lambda$, $b_\lambda$ and $c_\lambda$.

TABLE II
COEFFICIENTS OF THE MEAN AND STANDARD DEVIATION OF THE BEST
LOG-NORMAL FIT OF THE CFR AMPLITUDE

| Parameter ($\lambda$) | $a_\lambda$ | $b_\lambda$ | $c_\lambda$ ($\times 10^{-3}$) |
|---|---|---|---|
| $\mu$ | 0.537 | $-0.496$ | 1.512 |
| $\sigma$ | 0.445 | $-0.256$ | $-25.574$ |

In terms of mean value, the channel attenuation, in linear scale, increases exponentially with frequency, confirming that the power line cables have a low pass behavior. In terms of standard deviation, the channel statistics is less spread at higher frequencies.

Finally, the analysis of the phase of the CFR reveals that it can be modeled as uniformly distributed in $(-\pi, \pi)$ for each sample of the entire frequency range.

### B. Line Impedance

The characterization of the line impedance is important for the design of the analog front-end of the transmitter modem. The line impedance spreads over a broad set of values across the 1.8–100 MHz spectrum. Fig. 3 shows the 20-th, 50-th and 80-th percentile of both the resistive and reactive component of the line impedance. The best polynomial fit is also shown and it reads $q_{\lambda,\alpha} = a_{\lambda,\alpha} m^2 + b_{\lambda,\alpha} m + c_{\lambda,\alpha}$, where $q_{\lambda,\alpha}$ is the percentile at value $\alpha$ of the quantity $\lambda = \{R, X\}$, and $a_{\lambda,\alpha}$, $b_{\lambda,\alpha}$ and $c_{\lambda,\alpha}$ are constant parameter values. Table III reports the values of the coefficients. Basically, the resistive component is less spread at high frequencies and the lowest value increases with frequency. Indeed, the reactive quantiles
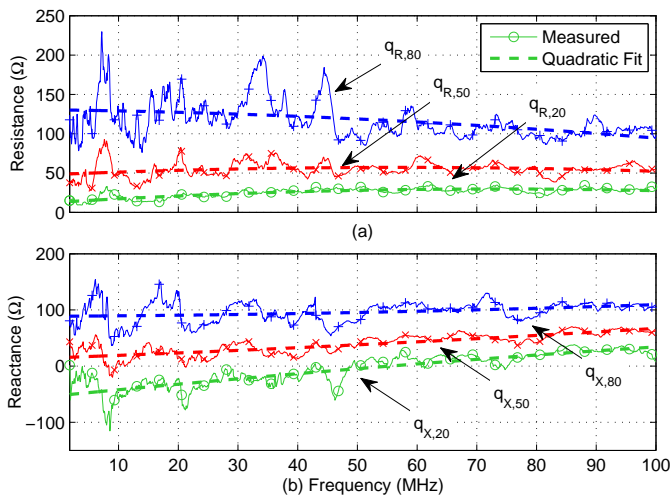
Fig. 3. 20-th, 50-th and 80-th percentiles of the resistive and reactive part of the line impedance on top and bottom, respectively. The best polynomial fit is also shown.
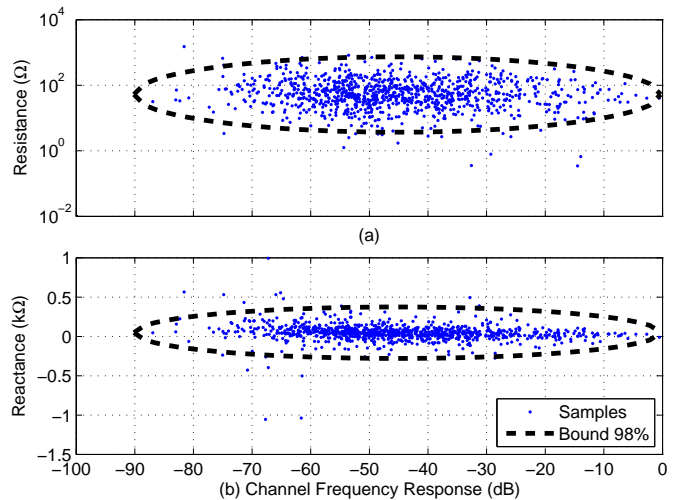


Fig. 4. Scatter plot of the resistive (on top) and the reactive (on bottom) component of the line impedance versus the CFR. The high-density regions are also shown.

exhibit a frequency increasing behavior, that turns into an inductive like nature.

TABLE III
QUADRATIC FITTING PARAMETER VALUES OF THE LINE IMPEDANCE COMPONENTS

| $\lambda$ | $\alpha$ | $a_{\lambda,\alpha}$ ($\Omega$) | $b_{\lambda,\alpha}$ ($\Omega$) | $c_{\lambda,\alpha}$ ($\Omega$) |
|---|---|---|---|---|
| | 20 | -1.213e-5 | 0.029 | 12.926 |
| $R$ | 50 | -1.053e-5 | 0.019 | 48.303 |
| | 80 | -1.004e-5 | -0.006 | 130.229 |
| | 20 | -7.045e-6 | 0.065 | -52.387 |
| $X$ | 50 | 5.036e-6 | 0.024 | 15.118 |
| | 80 | 5.705e-6 | 0.004 | 88.825 |

Furthermore, it is interesting to see whether the line impedance is related to the CFR. Fig. 4 shows the scatter plot of the line impedance components versus the CFR. The plot has been obtained gathering the samples from all frequencies. Despite the high variability, we identify high-density regions to which 98% of the samples belong. The region borders are shown in the figure. Similar results can be obtained by applying the same analysis frequency by frequency.

The target frequency range is 1.8–100 MHz, and the considered quantities are the dB-version of the amplitude of the CFR, the logarithmic representation of the resistive component of the line impedance and the reactive component in linear scale. The resistive part is considered in logarithmic scale in order to magnify the behavior for lower values, while the reactive part is in k$\Omega$. From the experimental evidence, the border of the high density region can be modeled as an ellipse that reads

$$\frac{(x-m_x)^2}{u^2} + \frac{(y-m_y)^2}{w^2} = 1, \qquad (11)$$

where $x$ and $y$ are the variables denoting the CFR and the line impedance component values, respectively. All other terms are constant coefficients. The parameter $m_x$ is the mean value of the measured CFR in dB. Similarly, $m_y$ is the mean of the impedance component, i.e., $m_y = E_{i,m}[\log_{10}(R^i(m))]$ for the resistance, and $m_y = E_{i,m}[X^i(m)/10^3]$ for the
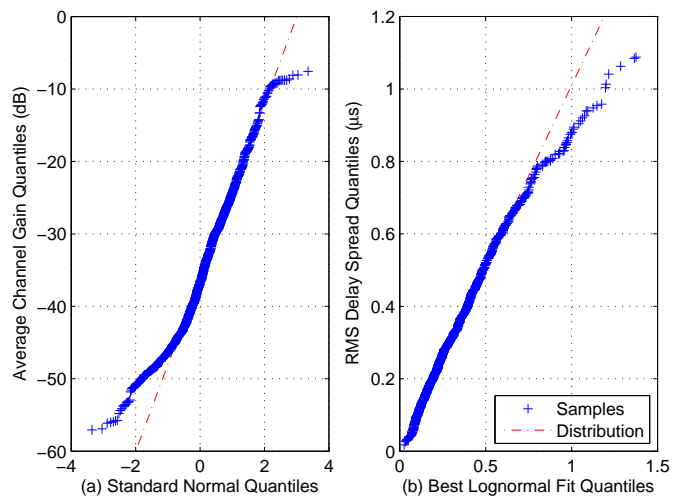


Fig. 5. On the left, scatter plot of the average channel gain versus the standard normal quantiles. On the right, scatter plot of the RMS delay spread versus the quantiles of the best Log-normal fit.

reactance. The expectation is done across frequencies and channel realizations. The remaining coefficients in (11) are obtained as follows.

According to the results of Section V-A, the dB version of the CFR is normally distributed with good approximation. For a normally distributed random variable, more than 99% of the samples are within three times the standard deviation. In this respect, $u = 3\sigma_x$, where $\sigma_x$ is the standard deviation of the CFR. Substituting $m_x$, $m_y$ and $u$ in (11) with the values described above, $w$ reads

$$w = \sqrt{\frac{u^2(y-m_y)^2}{u^2-(x-m_x)^2}}. \qquad (12)$$

Relation (12) can be computed for all $x$ and $y$. The result is a set of values of $w$, namely, $\mathbf{w}$. The value of the model of $w$ is chosen as the 98-th percentile of the cumulative distribution function (CDF) of $\mathbf{w}$. Table IV reports the values of the
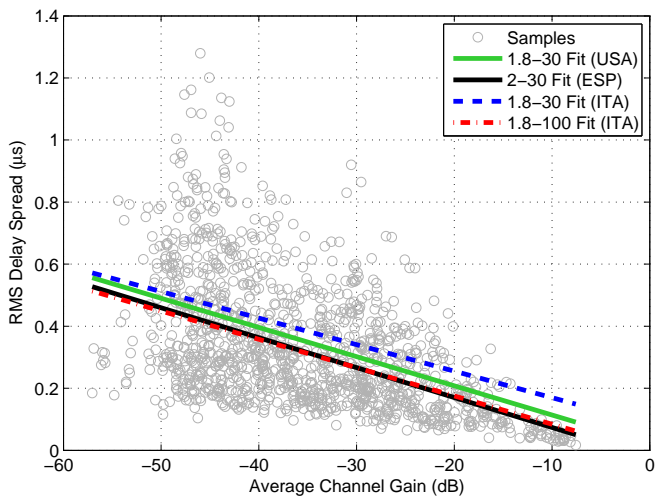
Fig. 6. RMS delay spread versus average channel gain and robust regression fit for both the bands 1.8–30 and 1.8–100 MHz. The 2–30 MHz Spanish (ESP) [12] and 1.8–30 MHz USA [11] robust regression fits are also shown.
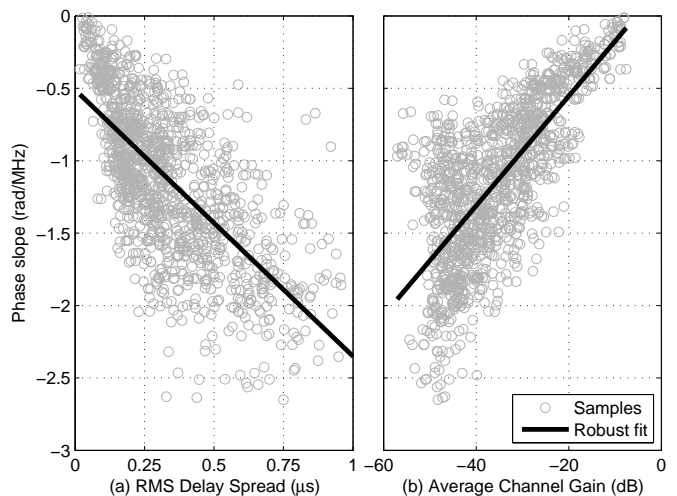


Fig. 7. On the left, scatter plot of phase slope versus delay spread. On the right, phase slope versus average channel gain. The robust regression fit is also shown.

constant coefficients in (11) for the resistive and the reactive component. Clearly, $m_x$ and $u$ are identical in both cases.

TABLE IV
PARAMETERS OF THE HIGH-DENSITY REGIONS

| Component | $m_x$ (dB) | $u$ (dB) | $m_y$ | $w$ |
|---|---|---|---|---|
| $R$ | $-45.236$ | $44.920$ | $1.718$ | $1.150$ |
| $X$ | | | $0.047$ (k$\Omega$) | $327.234$ (k$\Omega$) |

### C. Statistical Metrics

Firstly, let us focus on the ACG. Fig. 5a shows the quantiles of the ACG (in dB scale) versus the standard normal quantiles. The following observations can be made. First, the ACG ranges between $-7.6$ dB and $-57$ dB. The mean and the standard deviation, namely, $(\mu, \sigma)$, of the best normal fit of the ACG read $(-35.412, 10.521)$ dB, respectively. Furthermore, most of the samples lie on the dash-dotted line. This would suggest the ACG to be normally distributed though the normality is not strictly confirmed by tests that we have performed on the measured data, as Kolmogorov-Smirnov, that reject always the null hypotesis.

Now, let us focus on the RMS delay spread. Fig. 5b shows the quantiles of the measured delay spread versus the quantiles of the Log-normal distribution that provides the best fit. Most of the samples are closed to the dash-dotted line. This confirms that the RMS delay spread is log-normally distributed with good approximation, as pointed out in [11]. The mean and the standard deviation of the best Log-normal fit are $(0.346, 0.260)$ $\mu$s, but these values are strongly a function of the CIR computation method, as shown in Section III-A.

The relation between the RMS delay spread and the ACG of the measured channels is shown in Fig. 6. Basically, Fig. 6 is the scatter plot of the RMS delay spread as a function of the ACG (in dB scale). The robust fit is also reported. The two quantities are negatively related. In [11] and [12],

a similar study was performed for two sets of experimental data. The former is the result of a measurement campaign in the United States (USA) for the 1.8–30 MHz band. The latter, in Spain (ESP) for the 2–30 MHz band. Now, in order to compare the results, in Fig. 6, the robust regression fit of our data in the 1.8–30 MHz frequency range is also shown. A good agreement, especially with the ESP case, can be observed. Slight deviations of the lines slope and $y$-intercept may be due to the different frequency range, and differences on the procedure adopted to compute the CIR, that are reflected on the value of the RMS delay spread. The robust fit parameters, for each frequency band and scenario, are listed in Table V.

Fig. 7 shows the relation between the phase slope, the ACG and the delay spread. The phase slope is defined as the slope of the robust fit of the unwrapped phase of the CFR. The phase slope brings some information on the delay introduced by the channel and thus on the length of the backbone, namely, the shortest electrical path between the transmitter and the receiver. The delay increases with the distance of the path followed by the signal toward the receiver. Similarly, the channel attenuation is supposed to increase with the distance

TABLE V
ROBUST FIT PARAMETERS FOR THE RMS DELAY SPREAD VERSUS THE ACG IN DB SCALE [11], [12]

| Country | Band (MHz) | slope ($\times 10^{-3}$) ($\mu$s/dB) | $y$-intercept ($\mu$s) |
|---|---|---|---|
| USA | 1.8–30 | $-9.400$ | $0.020$ |
| ESP | 2–30 | $-9.630$ | $-0.022$ |
| ITA | 1.8–30 | $-8.545$ | $0.084$ |
| ITA | 1.8–100 | $-9.129$ | $-0.007$ |

TABLE VI
ROBUST FIT PARAMETERS FOR ACG AND DELAY SPREAD VERSUS THE PHASE SLOPE

| Metric | slope | | $y$-intercept | |
|---|---|---|---|---|
| $G$ | $0.038$ | (rad/(MHz $\cdot$ dB)) | $0.203$ | (rad / MHz ) |
| $\sigma_\tau$ | $-1.842$ | (rad/(MHz $\cdot$ $\mu$s )) | $-0.510$ | (rad / MHz) |
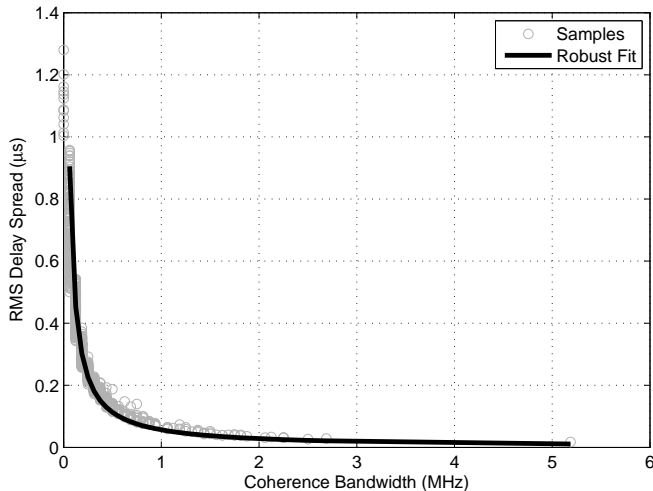
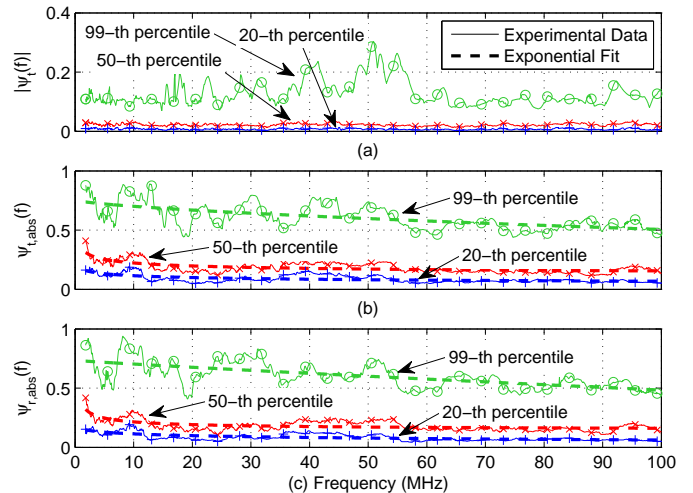Fig. 8. RMS delay spread versus coherence bandwidth and hyperbolic fit.



Fig. 9. 20-th, 50-th and 99-th percentile of the spatial correlation $|\psi_t(f)|$ (a), $\psi_{t,abs}(f)$ (b) and $\psi_{r,abs}(f)$ (c) as a function of frequency. For $\psi_{t,abs}(f)$ and $\psi_{r,abs}(f)$, the best exponential fit is also shown.

due to the effect of the non ideal cables and the impact of the branches connected to the backbone. This observation is validated by the results. Furthermore, Fig. 7a shows the relation between the RMS delay spread and the phase slope. The robust fit parameters for both the ACG and the RMS delay spread versus the phase slope are listed in Table VI.

Finally, let us focus on the correlation function and the CB. From the analysis of the statistical correlation function of the experimental data, we have verified that $\phi(\ell, m)$ does not depend only on the difference $\ell - m$. Therefore, the uncorrelated scattering assumption does not hold true. The presence of correlated scattering can be justified by the fact that reflections share the same signal path, namely, the backbone. Fig. 8 shows the relation between the deterministic CB $B_c^{0.9}$ and the RMS delay spread of the measured channels. The focus is on $B_c^{0.9}$ for consistency with previous analysis [9]. The samples are distributed according to a hyperbolic trend that reads

$$B_c^{0.9} = \frac{0.057}{\sigma_\tau} \quad \text{[Hz]}. \tag{13}$$

A similar result was pointed out in [9], for a set of channels measured in France. In detail, in [9], it was shown that the relation $B_c^{0.9}\sigma_\tau = 0.055$ holds, which is very close to (13).

Finally, Table VII shows the comparison between $\overline{B}_c^\rho$ and $\hat{B}_c^\rho$. The average deterministic CB $\overline{B}_c^\rho$ is closer to the statistical CB $\hat{B}_c^\rho$ for higher values of $\rho$ where they can be, to some extent, interchanged. This result can be exploited to fit the model in [14].

TABLE VII
COMPARISON AMONG THE STATISTICAL AND THE MEAN DETERMINISTIC
CB FOR DIFFERENT VALUES OF $\rho$

| $\rho$ | $\overline{B}_c^\rho$ (MHz) | $\hat{B}_c^\rho$ (MHz) |
|---|---|---|
| 0.9 | 0.288 | 0.438 |
| 0.8 | 0.545 | 0.938 |
| 0.7 | 0.846 | 1.563 |

### D. Spatial Correlation

The spatial correlation between channels of the same site has been found to be small, say, always below 0.06 in absolute value, regardless of the considered site or frequency. This result reflects the large variability of the in-home PLC scenario so that in average the channels are not correlated.

Nevertheless, if a spatial constraint were added, a higher correlation might be found. To dig further into this, we compute the correlation between channels that share the same transmitter, i.e., $\psi_t(m)$. Fig. 9 shows the profiles of the 20-th, 50-th and 99-th percentile of the CDF of the absolute value of $\psi_t(m)$ as a function of frequency. The maximum value of $|\psi_t(m)|$ is one order of magnitude larger than $|\psi(\ell, m)|$. Therefore, as intuition suggests, the correlation between channels that share the same transmitter outlet is non-negligible.

Now, let us focus on the correlation between the amplitude of the pair of CFRs, namely $\psi_{t,abs}(m)$. Fig. 9b shows the correspondent profiles for the same percentile values considered previously. Note that, by definition, $\psi_{t,abs}(m)$ is a real quantity. Interestingly, the correlation is large. Therefore, the low values experienced by $\psi_t(m)$ are due to the random phase of the channels. Furthermore, $\psi_{t,abs}(m)$ decreases as the frequency increases. Similar results are found for the correlation between the channels that share the receiver outlet, as shown in Fig. 9c, where we plot the percentiles, as in Fig. 9b, of $\psi_{r,abs}(m)$.

The experimental profiles of $\psi_{t,abs}(m)$ and $\psi_{r,abs}(m)$ can be fitted with an exponential function $\psi(m) = a\, m^b + c$, whose parameters are reported in Table VIII. The fitting profiles are shown in Figs. 9b-c.

### E. Maximum Achievable Rate

Firstly, we aim to study the relation between the maximum achievable rate and the distance, namely, we infer the achievable coverage. In this respect, we compute the maximum achievable rate of all channels and we perform the robust
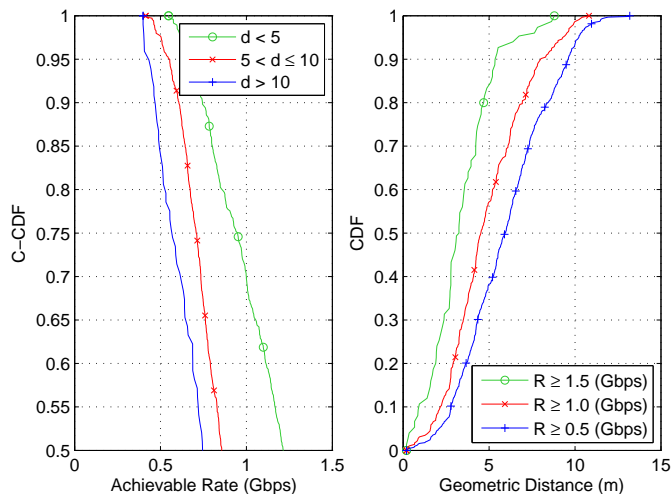
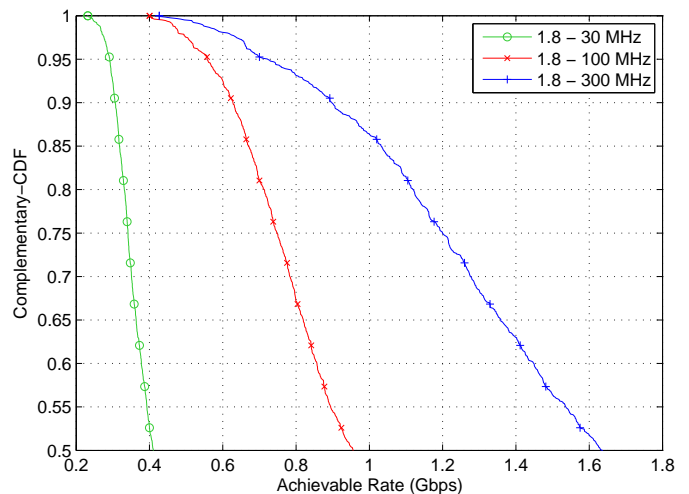Fig. 10. On the left, C-CDF of the achievable rate conditioned on the distance. On the right, CDF of the distance conditioned on the achievable rate.



Fig. 11. Complementary cumulative distribution function of the achievable rate for three different transmission bands.

fit as a function of the distance. Interestingly, the achievable rate decreases with the geometrical distance. The slope of the robust regression fit reads -70.153 kbps/m. To further infer coverage, we compute the complementary cumulative distribution function (C-CDF) of the maximum achievable rate conditioned on the distance. Fig. 10a shows the results for three values of distance. A similar result was already shown in [25], and differences in the maximum achievable rate values are amenable to the different noise model and transmitted PSD level. In 70% of the cases, only the channels associated to distances between outlets shorter than 5 m exceed 1 Gbps. In a dual manner, in Fig. 10b, we plot the CDF of the geometrical distance conditioned by the fact that the maximum achievable rate of the channel is larger than 0.5, 1, and 1.5 Gbps. Interestingly, data rates larger than 1.5 Gbps can be achieved with high probability only by channels shorter than 5 m. Therefore, in the considered sites, PLC can provide a real good option for very high speed connectivity between outlets that are nearly placed.

Now, we infer the improvement provided by the band extension beyond 100 MHz. We consider the channel measures acquired in a wider spectrum up to 300 MHz. To this aim, the noise model in (8) is extended up to 300 MHz and the transmitted PSD beyond 30 MHz is let be equal to $-80$ dBm/Hz. As a result, Fig. 11 shows the C-CDF profiles, and Tab. IX reports the 20-th, 50-th and 80-th percentile of the CDF of the achievable rate. The maximum achievable rate improves significantly, but the increase provided by the bandwidth enlargement is not proportional to such a bandwidth extension. In this respect, let us define the spectral efficiency $\eta$ as the ratio between the maximum achievable rate and the transmission bandwidth. Table IX reports the spectral efficiency coefficient for the three cases. As it can be noted, on average, the spectral efficiency decreases as the bandwidth increases. This is due to the large attenuation exhibited by the PLC channels at very high frequencies.

## VI. CONCLUSIONS

A statistical characterization of the in-home PLC channel has been presented from a set of measures acquired in Italy. The analysis brings new insights on the channel behavior, and further it confirms some prior results presented in the literature that were obtained from measurements in other countries. We aim to allow a precise comparison between the results of this analysis and those from other campaigns. In this respect, we have pointed out the need of common processing procedures and the importance of using the same definition of the physical quantities to be analyzed. In this respect, we have detailed a procedure to compute the channel impulse response as well as we have made available an on-line script that implements the procedure and that computes the average channel gain, the RMS delay spread, and the deterministic coherence bandwidth. It is intended to be used for the analysis of the results of future measurement campaigns, providing results that are consistent with the ones herein presented. Besides the processing procedures, we have carried out a statistical analysis whose findings can be summarized as follows.

TABLE VIII
PARAMETER VALUES OF THE BEST EXPONENTIAL FIT OF THE QUANTILES OF $\psi_{t,abs}(m)$ AND $\psi_{r,abs}(m)$

| Correlation | Percentile | $a$ | $b$ | $c$ |
|---|---|---|---|---|
| $\psi_{t,abs}(m)$ | 99-th | $-1.873 \times 10^{-3}$ | 0.663 | 0.755 |
| | 50-th | 0.602 | $-0.290$ | 0.085 |
| | 20-th | 0.357 | $-0.119$ | $-0.080$ |
| $\psi_{r,abs}(m)$ | 99-th | $-0.315 \times 10^{-3}$ | 0.906 | 0.735 |
| | 50-th | 0.981 | $-0.496$ | 0.136 |
| | 20-th | $-0.274$ | 0.057 | 0.480 |

TABLE IX
ACHIEVABLE RATE PERCENTILES, AND MEAN SPECTRAL EFFICIENCY FOR THREE TRANSMISSION BANDS

| Band (MHz) | 20-th (Mbps) | 50-th (Mbps) | 80-th (Mbps) | $\eta$ (bps/Hz) |
|---|---|---|---|---|
| 1.8–30 | 331 | 410 | 525 | 15.27 |
| 1.8–100 | 714 | 956 | 1282 | 10.47 |
| 1.8–300 | 1121 | 1637 | 2721 | 6.50 |

- The PLC channel is significantly frequency selective in the band 1.8-100 MHz. The magnitude of the channel frequency response is "quasi" Log-normal, i.e., the Log-normal distribution applies to most but not all the frequency samples that we considered. The log-normality applies also to the RMS delay spread, while the average channel gain (in dB) is normally distributed with good approximation. This confirms previous results obtained in other measurement campaigns. Furthermore, the parameters of the best fit of such quantities and of the robust regression fit of their relations have been described analytically.

- The hyperbolic relation between the coherence bandwidth and the RMS delay spread has been described analytically. The differences between two coherence bandwidth definitions, namely the statistical CB and the deterministic CB, have been discussed.

- The line impedance in the range 1.8-100 MHz can assume a broad set of values but, in general, the spread is more pronounced in the lower frequency range. Furthermore, the analysis of the reactive component highlights an inductive behavior.

- No clear relation between the line impedance and the channel frequency response has been identified. However, the scatter plot of the line impedance components versus the channel frequency response (in dB) highlights a high probability region that can be analytically described.

- The spatial dependency of the channels has been analyzed. The overall ensemble of pair of channels belonging to a given site is essentially uncorrelated. However, if we constrain the pair of channels to be associated to the same transmitter (broadcast channel), then a more pronounced correlation is found. Furthermore, a larger correlation is found if the latter study is limited to the amplitude of the channel frequency response. It follows that the random phase reduces significantly the spatial correlation. Similar results apply to the channels that share the receiver outlet.

- The in-home wiring connecting a pair of outlets can follow "unpredictable" paths, so that the electrical and the geometrical distances do not coincide. Nevertheless, the geometrical distance between two outlets can be statistically related to the maximum achievable rate. This allows to infer the coverage offered by PLC systems. In the tested scenario, rates in excess of 1 Gbps can be sustained only between outlets at distances smaller than 5 m. This application scenario is not uncommon, e.g., the connectivity between a set-top box and a TV.

- Signaling above 100 MHz (and in particular up to 300 MHz) can provide achievable rate improvements. However, the spectral efficiency, i.e., the bit rate per-unit-frequency, decreases significantly.

## REFERENCES

[1] M. Schwartz, "Carrier-Wave Telephony over Power Lines: Early History," *IEEE Commun. Mag.*, vol. 47, no. 1, pp. 14–18, Jan. 2009.

[2] L. Yonge, J. Abad, K. Afkhamie, L. Guerrieri, S. Katar, H. Lioe, P. Pagani, R. Riva, D. M. Schneider, and A. Schwager, "An Overview of the HomePlug AV2 Technology," *Journal of Electrical and Computer Engineering*, vol. 2013, pp. 1–20, 2013.

[3] M. Zimmermann and K. Dostert, "A Multipath Model for the Powerline Channel," *IEEE Trans. Commun.*, vol. 50, no. 4, pp. 553–559, Apr. 2002.

[4] D. Liu, E. Flint, B. Gaucher, and Y. Kwark, "Wide Band AC Power Line Characterization," *IEEE Trans. Consum. Electron.*, vol. 45, no. 4, pp. 1087 – 1097, Nov. 1999.

[5] B. O'Mahony, "Field Testing of High Speed Power Line Communications in North American Homes," in *Proc. IEEE Int. Symp. Power Line Commun. and Its App. (ISPLC)*, Mar. 2006, pp. 155–159.

[6] IEEE Standard for Broadband Over Power Line Networks: Medium Access Control and Physical Layer Specifications. IEEE Std. 1901-2010, Sep. 2010.

[7] Unified High-Speed Wireline-Based Home Networking Transceivers - System Architecture and Physical Layer Specification. ITU-T Rec. G.9960, Dec. 2011. [Online]. Available: https://www.itu.int/rec/T-REC-G.9960/en

[8] M. Tlich, A. Zeddam, A. Moulin, and F. Gauthier, "Indoor Power-Line Communications Channel Characterization Up to 100 MHz - Part I: One-Parameter Deterministic Model," *IEEE Trans. Power Del.*, vol. 23, no. 3, pp. 1392–1401, Jul. 2008.

[9] M. Tlich, A. Zeddam, A. Moulin, and F. Gauthier, "Indoor Power-Line Communications Channel Characterization up to 100 MHz - Part II: Time-Frequency Analysis," *IEEE Trans. Power Del.*, vol. 23, no. 3, pp. 1402–1409, Jul. 2008.

[10] S. Galli, "A Simplified Model for the Indoor Power Line Channel," in *Proc. IEEE Int. Symp. Power Line Commun. and Its App. (ISPLC)*, Apr. 2009, pp. 13–19.

[11] S. Galli, "A Novel Approach to the Statistical Modeling of Wireline Channels," *IEEE Trans. Commun.*, vol. 59, no. 5, pp. 1332–1345, May 2011.

[12] J. A. Cortés, F. J. Cañete, L. Díez, and J. L. G. Moreno, "On the Statistical Properties of Indoor Power Line Channels: Measurements and Models," in *Proc. Int. Symp. Power Line Commun. and Its App. (ISPLC)*, Apr. 2011, pp. 271–276.

[13] H. Phillips, "Modelling of Powerline Communication Channels," in *Proc. IEEE Int. Symp. Power Line Commun. and Its App. (ISPLC)*, Mar. 1999, pp. 14–21.

[14] A. M. Tonello, F. Versolatto, B. Béjar, and S. Zazo, "A Fitting Algorithm for Random Modeling the PLC Channel," *IEEE Trans. Power Del.*, vol. 27, no. 3, pp. 1477–1484, Jun. 2012.

[15] S. Galli, "A Simple Two-Tap Statistical Model for the Power Line Channel," in *Proc. Int. Symp. Power Line Commun. and Its App. (ISPLC)*, Mar. 2010, pp. 242–248.

[16] J. S. Barnes, "A Physical Multi-Path Model for Power Distribution Network Propagation," in *Proc. IEEE Int. Symp. Power Line Commun. and Its App. (ISPLC)*, Mar. 1998, pp. 76–89.

[17] O. G. Hooijen, "On The Relation Between Network-Topology and Power Line Signal Attenuation," in *Proc. Int. Symp. Power Line Commun. and Its App. (ISPLC)*, Mar. 1998, pp. 45–56.

[18] H. Meng, Y. L. Guan, C. L. Law, P. L. So, E. Gunawan, and T. Lie, "Modeling of Transfer Characteristics for the Broadband Power Line Communication Channel," *IEEE Trans. Power Del.*, vol. 19, no. 3, pp. 1057–1064, Jul. 2004.

[19] J. Anatory, N. Theethayi, and R. Thottappillil, "Power-Line Communication Channel Model for Interconnected Networks - Part I: Two-Conductor System," *IEEE Trans. Power Del.*, vol. 24, no. 1, pp. 118–123, Jan. 2009.

[20] S. Barmada, A. Musolino, and M. Raugi, "Innovative Model for Time-Varying Power Line Communication Channel Response Evaluation," *IEEE J. Sel. Areas Commun.*, vol. 24, no. 7, pp. 1317–1326, Jul. 2006.

[21] T. Esmailian, F. R. Kschischang, and P. Glenn Gulak, "In-Building Power Lines as High-Speed Communication Channels: Channel Characterization and a Test Channel Ensemble," *Intern. J. Commun. Syst.*, vol. 16, no. 5, pp. 381–400, Jun. 2003.

[22] S. Galli and T. C. Banwell, "A Deterministic Frequency-Domain Model for the Indoor Power Line Transfer Function," *IEEE J. Sel. Areas Commun.*, vol. 24, no. 7, pp. 1304–1316, Jul. 2006.

[23] A. M. Tonello and F. Versolatto, "Bottom-Up Statistical PLC Channel Modeling - Part I: Random Topology Model and Efficient Transfer Function Computation," *IEEE Trans. Power Del.*, vol. 26, no. 2, pp. 891–898, Apr. 2011.

[24] F. J. Cañete, J. A. Cortés, L. Díez, and J. T. Entrambasaguas, "A Channel Model Proposal for Indoor Power Line Communications," *IEEE Commun. Mag.*, vol. 49, pp. 166–174, Dec. 2011.

[25] F. Versolatto and A. M. Tonello, "On the Relation Between Geometrical Distance and Channel Statistics in In-Home PLC Networks," in *Proc. IEEE Int. Symp. Power Line Commun. and Its App. (ISPLC)*, Mar. 2012, pp. 280–285.

[26] F. Versolatto and A. M. Tonello, "PLC Channel Characterization up to 300 MHz: Frequency Response and Line Impedance," in *Proc. IEEE Global Commun. Conf. (GLOBECOM)*, Dec. 2012, pp. 3525–3530.

[27] From the PLC Channel Measurements to the Statistics: A Matlab Script. [Online]. Available: www.diegm.uniud.it/tonello

[28] F. J. Cañete, J. A. Cortés, L. Díez, and J. T. Entrambasaguas, "Analysis of the Cyclic Short-Term Variation of Indoor Power Line Channels," *IEEE J. Sel. Areas in Commun.*, vol. 24, no. 7, pp. 1327–1338, Jul. 2006.

[29] F. Gianaroli, F. Pancaldi, and G. M. Vitetta, "Broadband System Models Based on Zadeh's Representation for Indoor Powerline Channels: An Experimental Validation," in *Proc. IEEE Int. Conf. Commun. (ICC)*, Jun. 2013, pp. 2897–2902.

[30] J. Proakis, *Digital Communications*. McGraw - Hill, 2007.

[31] R. Hashmat, P. Pagani, and T. Chonavel, "MIMO Communications for Inhome PLC Networks: Measurements and Results up to 100 MHz," in *Proc. IEEE Int. Symp. Power Line Commun. and Its App. (ISPLC)*, Apr. 2010, pp. 120–124.

[32] B. Praho, M. Tlich, P. Pagani, A. Zeddam, and F. Nouvel, "Cognitive Detection Method of Radio Frequencies on Power Line Networks," in *Proc. IEEE Int. Symp. Power Line Commun. and Its App. (ISPLC)*, Apr. 2010, pp. 225–230.

[33] P. J. Bickel and K. A. Doksum, *Mathematical Statistics, Basic Ideas and Selected Topics*. Prentice Hall, 2001, vol. 1.
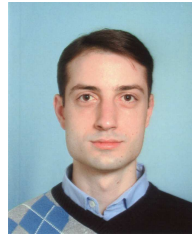
**Alberto Pittolo** received from the University of Udine, Udine, Italy, the Laurea degree in electrical engineering (2009) and the Laurea Specialistica degree (2012) in electrical and telecommunications engineering, with honors. He is currently pursuing the Ph.D. His research interests and activities are channel modeling and physical layer security for both wireless and power line communications.

**Andrea M. Tonello** (M'00–SM'12) is an Aggregate Professor at the University of Udine, Italy (since 2003) where he leads the Wireless and Power Line Communication Lab. He is also the founder of WiTiKee, a university spin-off company working in the field of telecommunications for the smart grid. From 1997 to 2002 he has been with Bell Labs Lucent Technologies firstly as a Member of Technical Staff and then as a Technical Manager at the Advanced Wireless Technology Laboratory, Whippany, NJ and the Managing Director of the Bell Labs Italy division. He obtained the Laurea degree (1996) and the Doctor of Research degree in electronics and telecommunications (2003) from the University of Padova, Italy. Dr. Tonello received the Full Professor Habilitation in 2013 and several recognitions among which the Lucent Bell Labs Recognition of Excellence (1999), the Distinguished Visiting Fellowship from the Royal Academy of Engineering, UK (2010) and the Distinguished Lecturer Award by the IEEE Vehicular Technology Society (2011-15). He also received (as co-author) five best paper awards. He serves/ed as an Associate Editor for the IEEE Transactions on Vehicular Technology (2007-2013), for the IEEE Transactions on Communications (since 2012) and IEEE Access (since 2013). He served as the general chair of IEEE ISPLC 2011 and he is the general co-chair of IEEE SmartGridComm 2014. He is the Chair of the IEEE Communications Society Technical Committee on Power Line Communications.

**Fabio Versolatto** (GSM'10) received the Laurea degree (2007) and the Laurea Specialistica degree (2009) in electrical engineering (both summa cum laude), and the Ph.D. degree in industrial and information engineering (2013), from the University of Udine, Udine, Italy. Currently, he is member of the Wireless and Power Line Communications Lab (WiPLi Lab) at the University of Udine, and his research interests are in the field of channel modeling for power line communications and digital communication algorithms.

He is member of the IEEE Technical Committee on Power Line Communications (TC-PLC). He received the best student paper award at the IEEE Int. Symp. on Power Line Commun. and Its App. 2010.